We are IntechOpen,
the world's leading publisher of
Open Access books
Built by scientists, for scientists

4,800
Open access books available

122,000
International authors and editors

135M
Downloads

Our authors are among the

154
Countries delivered to

TOP 1%
most cited scientists

12.2%
Contributors from top 500 universities

WEB OF SCIENCE™

Selection of our books indexed in the Book Citation Index
in Web of Science™ Core Collection (BKCI)

Interested in publishing with us?
Contact book.department@intechopen.com

Numbers displayed above are based on latest data collected.
For more information visit www.intechopen.com

Interference Alignment for UWB-MIMO Communication Systems

Mohamed El-Hadidy, Mohammed El-Absi, Yoke Leen Sit, Markus Kock, Thomas Zwick, Holger Blume and Thomas Kaiser

1. Introduction

Due to the enormous occupied bandwidth even by a single pair of UWB users, one major scientific challenge in UWB communications is interference management. Recently, Interference Alignment (IA) has become popular not only to well manage the interference, but also to optimally exploit the possible capacity gain caused by multiple pairs of transmitters and receivers. Theoretically, IA scales the channel capacity by $K/2$, where K is the number of user pairs. This fact makes IA highly attractive for future communication systems with numerous pairs of users. However, in the literature it has been reported that IA is not robust [7] against imperfections such as channel estimation errors. Thanks to the interdisciplinary research of antenna, communication and hardware engineers within the UKoLoS project *Decimus*, we were able to jointly search for solutions to improve IA robustness while not suffering from too perfect simulation idealities or too unrealistic hardware requirements. We find that *antenna* or *pattern selection* is a promising approach to improving the robustness of IA while keeping the underlying algorithms at a reasonable complexity and feasibility for implementation. Our contribution is structured as follows: first, a brief introduction of IA tailored to UWB is given. Then, we propose an antenna selection algorithm with low complexity and demonstrate its performance. In the third chapter a general methodology of MIMO UWB antenna design for orthogonal channels maximizing the channel capacity is presented. A first outcome of this methodology is a multi-mode orthogonal antenna which has been used for the investigated antenna selection approach. At last, the hardware requirements of IA systems with the proposed antenna selection method are studied. A conclusion summarizes the outcomes of our contribution.

2. MIMO-UWB interference mitigation by interference alignment

IA is a promising technique which achieves the maximum degrees of freedom (DoF) for K users in interference channels [4]. This can be achieved by a combination of linear precoding

at the transmitters and interference suppression at the receivers. IA permits to force interfering signals at each receiver in one subspace and the desired signal in another orthogonal subspace [5].

Consider a K-user UWB Multi Band Orthogonal Frequency Division Multiplexing (MB-OFDM) interference channel with M_j transmit antennas at transmitter j and N_i receive antennas at receiver i. All users transmit d_s streams using N sub-carriers. Every transmitter communicates with his desired receiver and causes interference to other pairs of transmitter and receiver. The discrete-time complex received signal over the nth subcarrier at the ith receiver over a flat channel is represented as[21],[28]:

$$\mathbf{y}_i^n = \sum_{j=1}^{K} \mathbf{H}_{ij}^n \mathbf{V}_j^n \mathbf{x}_j^n + \mathbf{z}_i^n = \mathbf{H}_{ii}^n \mathbf{V}_i^n \mathbf{x}_i^n + \sum_{j=1,j\neq i}^{K} \mathbf{H}_{ij}^n \mathbf{V}_j^n \mathbf{x}_j^n + \mathbf{z}_i^n \tag{1}$$

where $\mathbf{y}_i^n$ is the $N_i \times 1$ received vector at receiver i, $\mathbf{H}_{ij}^n$ is the $N_i \times M_j$ flat frequency domain channel matrix over nth subcarrier between jth transmitter and ith receiver, $\mathbf{V}_j^n$ is the $M_j \times d_s$ unitary precoding matrix which is applied for the transmitted $M_j \times 1$ vector $\mathbf{x}_j^n$ from the jth transmitter, and $\mathbf{z}_i^n$ is the $N_i \times 1$ zero mean unit variance circularly symmetric additive white Gaussian noise vector at receiver i. The Channel State Information (CSI) is assumed to be perfectly known at each node. To reconstruct the transmitted d_s signal at the ith receiver, the received signal is decoded using a unitary linear suppression interference matrix $\mathbf{U}_i^n$. The reconstructed data $\widehat{\mathbf{y}}$ at receiver i is defined as:

$$\widehat{\mathbf{y}}_i^n = \mathbf{U}_i^{nH} \mathbf{H}_{ii}^n \mathbf{V}_i^n \mathbf{x}_i^n + \sum_{j=1,j\neq i}^{K} \mathbf{U}_i^{nH} \mathbf{H}_{ij}^n \mathbf{V}_j^n x_j^n + \mathbf{U}_i^{nH} \mathbf{z}_i^n \tag{2}$$

For perfect interference alignment, the following conditions need to be fulfilled [1]:

$$\text{rank}\left(\mathbf{U}_i^{nH} \mathbf{H}_{ii}^n \mathbf{V}_i^n\right) = d_s \qquad \forall i \tag{3}$$

and

$$\mathbf{U}_i^{nH} \mathbf{H}_{ij}^n \mathbf{V}_j^n = 0 \qquad \forall j \neq i \tag{4}$$

According to (3) and (4), the received signal after processed by the linear suppression interference matrix is:

$$\widehat{\mathbf{y}}_i^n = \mathbf{U}_i^{nH} \mathbf{H}_{ii}^n \mathbf{V}_i^n \mathbf{x}_i^n + \mathbf{U}_i^{nH} \mathbf{z}_i^n \tag{5}$$

2.1. Closed-form interference alignment

In order to achieve a closed-form IA solution, 3 users interference channel (K=3) has been considered, where each node has $M = 2d$ antennas, and each user wishes to achieve d degrees of freedom by applying the IA principles. The conditions of IA given in (3) and (4) are obtained by setting the precoding matrices as [4]:

$$\mathbf{V}_1 = \text{eign}(\mathbf{H}_{31}^{-1} \mathbf{H}_{32} \mathbf{H}_{12}^{-1} \mathbf{H}_{13} \mathbf{H}_{23}^{-1} \mathbf{H}_{21}) \tag{6}$$

$$\mathbf{V}_2 = (\mathbf{H}_{32}^{-1} \mathbf{H}_{31} \mathbf{V}_1) \tag{7}$$

$$\mathbf{V}_3 = (\mathbf{H}_{23}^{-1} \mathbf{H}_{21} \mathbf{V}_1) \tag{8}$$

and the interference suppression matrix for receiver i is given by:

$$\mathbf{U}_i = \text{null}([\mathbf{H}_{ij}\mathbf{V}_j]) \qquad \forall j \neq i \tag{9}$$
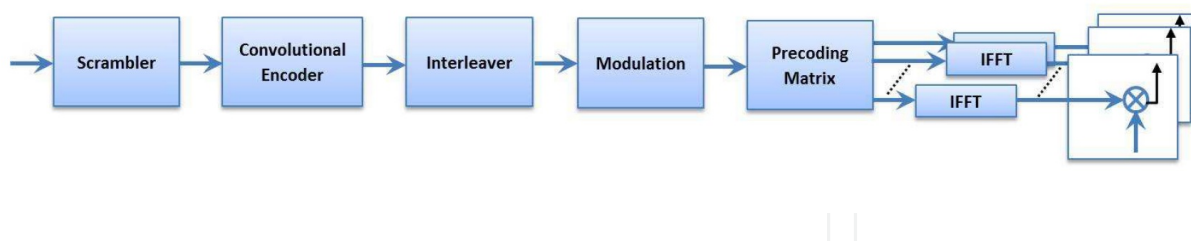

Figure 1. Transmitter block diagram of a MIMO UWB MB-OFDM communication system.

2.2. Artificial channel diversity algorithm

For successful applying the IA principle a sufficient orthogonality between all channels is required. In real-world indoor environments and MIMO UWB systems such orthogonality is not guaranteed; instead, the small distances between neighboring antennas and a possible low scattering could lead to high correlation among the several channels of the communication system. Therefore, the orthogonal component of the desired signal to the plane of the aligned undesired signals would be less pronounced, leading to worse overall system performance and robustness.

To overcome this problem, an artificial channel diversity technique is applied utilizing an antenna selection algorithm. The goal of this algorithm is to maximize the *orthogonality* of the desired signal on the plane of the aligned undesired ones. Here each transmitting node has Q_i antennas and only the best M_i antennas will be selected for maximizing the orthogonality of the desired component on the undesired signals plane. A brut force iterative process is carried out for all available combinations to choose the best selection that realizes this maximum orthogonality [8]. In the next section, the antenna selection criteria are illustrated in more detail.

3. Low complexity signal processing antenna selection algorithm

As mentioned before we propose an antenna selection algorithm in order to increase the required orthogonality directly leading to a more robust communication system in terms of minimum Bit Error Rate (BER). Note that antenna selection is a widely known approach in order to capture diversity and to improve the SNR of the communication systems [19],[14].

3.1. Antenna selection criterion

In the following we consider a K-user MIMO system with perfect IA. The selection algorithm consists of choosing the best M out of the L available transmit antennas. Denote by S_k the selected subset indices of the transmit antennas of k users [6]. The goal of the selection is to find S_k for all users $\{k = 1 : K\}$ which maximizes the average SNR_S for the multi-user system by increasing the projected desired signal into the interference-free space. This can be achieved by minimizing the principal angles between the desired signal subspace and

the interference-free subspace. Minimizing the principal angles is equivalent to maximizing so-called *canonical correlations*.

Let ζ_1 and ζ_2 be subspaces in the complex plane $\mathbb{C}$. Considering the dimension of ζ_1 is smaller than or equal to the dimension of ζ_2 ($\dim \zeta_1 = d_1 \leqslant \dim \zeta_2 = d_2$). The canonical correlations are defined as the cosines of the principal angles between any two linear subspaces, which can uniquely defined as [3]

$$\cos \theta_i = \max_{\mathbf{a}_i \in \zeta_1} \max_{\mathbf{b}_i \in \zeta_2} \mathbf{a}_i^H \mathbf{b}_i, \qquad i = 1, ..., d_1, \tag{10}$$

where $\mathbf{a}_i$ and $\mathbf{b}_i$ are principal vectors of ζ_1 and ζ_2 respectively, subject to $\mathbf{a}_i^H \cdot \mathbf{a}_i = \mathbf{b}_i^H \cdot \mathbf{b}_i = 1$ and $\mathbf{a}_i^H \cdot \mathbf{a}_j = \mathbf{b}_i^H \cdot \mathbf{b}_j = 0$, $i \neq j$.

If $\mathbf{Q}_1$ and $\mathbf{Q}_2$ are orthonormal bases of the two subspaces ζ_1 and ζ_2 respectively, the canonical correlations are obtained as singular values of $\mathbf{Q}_1^H \mathbf{Q}_2 \in \mathbb{C}^{d_1 \times d_2}$ as follows [3]

$$\mathbf{Q}_1^H \mathbf{Q}_2 = \mathbf{P}_1 \Lambda \mathbf{P}_2^H \quad , \tag{11}$$

where $\mathbf{P}_1$ is a $d_1 \times d_1$ unitary matrix and $\mathbf{P}_2$ is a $d_2 \times d_2$ unitary matrix, Λ is is $d_1 \times d_2$ diagonal matrix with nonnegative real numbers on the diagonal. Therefore, $\Lambda = \mathrm{diag}(\alpha_1, .., \alpha_{d_1})$ and $\alpha_1, .., \alpha_{d_1}$ are the canonical correlations of the subspaces.

Observe that the principal angles are given by

$$\theta_i = \cos^{-1}(\alpha_i), \qquad i = 1, .., d_1. \tag{12}$$

In order to maximize the SNR at the receiver, the antenna selection criterion relies on maximizing the canonical correlations between $\mathbf{U}_k$ and $\mathbf{H}_{kk}\mathbf{V}_k$ as follows

$$S_k = \arg \min \angle (\mathbf{U}_k; \mathbf{H}_{kk}\mathbf{V}_k) \qquad ; k = 1, .., K \tag{13}$$

$$S_k = \arg \max \cos (\angle (\mathbf{U}_k; \mathbf{H}_{kk}\mathbf{V}_k)) \quad ; k = 1, .., K \tag{14}$$

$$S_k = \arg \max (\alpha_1, ..., \alpha_{d_s}) \qquad ; k = 1, 2, .., K, \tag{15}$$

where $(\alpha_1, ..., \alpha_{d_s})$ are the canonical correlations between subspace $\mathbf{U}_k$ and subspace $\mathbf{H}_{kk}\mathbf{V}_k$.

3.2. Relation between sum-rate and canonical correlations

The impact of the canonical correlations on the sum rate of a K-user MIMO system is given by [6]:

$$C = \sum_{k=1}^{K} \log \left| \mathbf{I}_N + \left(\sigma^2 \mathbf{I}_N + \sum_{l \neq k} \mathbf{W}_{kl} \right)^{-1} \mathbf{W}_{kk} \right|, \tag{16}$$

where C is the sum-rate, $\mathbf{W}_{kl} = \mathbf{H}_{kl}\mathbf{V}_l\mathbf{V}_l^H\mathbf{H}_{kl}^H$ denotes the $N \times N$ interference covariance matrix of the signal from the l-th transmitter to the k-th receiver, σ^2 is the variance of the additive white Gaussian noise, and $\mathbf{W}_{kk} = \mathbf{H}_{kk}\mathbf{V}_k\mathbf{V}_k^H\mathbf{H}_{kk}^H$ denotes the $N \times N$ covariance matrix of the desired signal. While perfect IA is assumed according to (3) and (4), the interference channel is equivalent to a set of parallel Gaussian MIMO channels, where the MIMO channel

transfer function is given by $\overline{\mathbf{H}}_k = \mathbf{U}_k^H \mathbf{H}_{kk} \mathbf{V}_k$, for $k = 1, .., K$. Then the sumrate equation in (16) reduces to

$$C = \sum_{k=1}^{K} \log \left| \mathbf{I}_N + \frac{1}{\sigma^2} \mathbf{U}_k^H \mathbf{H}_{kk} \mathbf{V}_k \mathbf{V}_k^H \mathbf{H}_{kk}^H \mathbf{U}_k \right|. \tag{17}$$

Note that at high SNR, (17) can be approximated as

$$C \simeq \sum_{k=1}^{K} \log \left| \frac{1}{\sigma^2} \mathbf{U}_k^H \mathbf{H}_{kk} \mathbf{V}_k \mathbf{V}_k^H \mathbf{H}_{kk}^H \mathbf{U}_k \right|, \tag{18}$$

and by applying a thin QR decomposition

$$\mathbf{U}_k = \mathbf{Q}_{U_k} \mathbf{R}_{U_k}, \tag{19}$$

where

$$\mathbf{H}_{kk} \mathbf{V}_k = \mathbf{Q}_{V_k} \mathbf{R}_{V_k} \tag{20}$$

and $\mathbf{Q}_{U_k}$, $\mathbf{Q}_{V_k}$ are orthonormal $N \times d_s$ matrix and $\mathbf{R}_{U_k}$, $\mathbf{R}_{V_k}$ are $d_s \times d_s$ upper triangle matrix it follows

$$C = \sum_{k=1}^{K} \log \left| \frac{1}{\sigma^2} \left(\mathbf{Q}_{U_k} \mathbf{R}_{U_k} \right)^H \left(\mathbf{Q}_{V_k} \mathbf{R}_{V_k} \right) \left(\mathbf{Q}_{V_k} \mathbf{R}_{V_k} \right)^H \left(\mathbf{Q}_{U_k} \mathbf{R}_{U_k} \right) \right|. \tag{21}$$

Since $\mathbf{U}_k$ is a unitary matrix, meaning $\left| \mathbf{R}_{U_k} \mathbf{R}_{U_k}^H \right| = 1$ it furthermore follows

$$C = \sum_{k=1}^{K} \log \left(\left(\frac{1}{\sigma^2} \right)^2 \left| \mathbf{Q}_{U_k}^H \mathbf{Q}_{V_k} \right| \left| \mathbf{Q}_{V_k}^H \mathbf{Q}_{U_k} \right| \left| \mathbf{R}_{V_k} \mathbf{R}_{V_k}^H \right| \right). \tag{22}$$

Since $\mathbf{Q}_{U_k}$ and $\mathbf{Q}_{V_k}$ are the orthonormal basis of the two subspaces $\mathbf{U}_k$ and $\mathbf{H}_{kk} \mathbf{V}_k$ respectively, (22) can be linked to the principal angles between the two subspace using (11). Therefore, (22) can be written as

$$C = \sum_{k=1}^{K} \log \left(\left(\frac{1}{\sigma^2} \right)^2 \left| \mathbf{P}_{k1} \Lambda \mathbf{P}_{k2}^H \right| \left| \mathbf{P}_{k2} \Lambda \mathbf{P}_{k1}^H \right| \left| \mathbf{R}_{V_k} \mathbf{R}_{V_k}^H \right| \right) \tag{23}$$

such that

$$\mathbf{Q}_{U_k}^H \mathbf{Q}_{V_k} = \mathbf{P}_{k1} \Lambda \mathbf{P}_{k2}^H,$$

where $\mathbf{P}_{k1}$ and $\mathbf{P}_{k2}$ are $d_s \times d_s$ unitary matrices and Λ is $d_s \times d_s$ diagonal matrix equals $\text{diag}(\alpha_1, .., \alpha_{d_s})$.

Thereafter, (22) can be re-formulated as

$$C = \sum_{k=1}^{K} \log \left(\left(\frac{1}{\sigma^2} \right)^2 \left(\prod_{i=1}^{d_s} \alpha_i \right)^2 \left| \mathbf{R}_{V_k} \mathbf{R}_{V_k}^H \right| \right), \tag{24}$$

where $(\alpha_1, ..., \alpha_{d_s})$ are the canonical correlations between subspace $\mathbf{U}_k$ and subspace $\mathbf{H}_{kk} \mathbf{V}_k$. From (23) it is shown that maximizing the canonical correlations increases C, but still does not result in the maximum C because the term $\left| \mathbf{R}_{V_k} \mathbf{R}_{V_k}^H \right|$ is linked to the matrix of coefficients participating in the linear combinations yielding the columns of $\mathbf{H}_{kk}$.

3.3. Simulation results analysis

All the following simulation results have been obtained based on real-world deterministic scenarios. The deterministic hybrid EM ray-tracing channel model was considered for the MIMO UWB channel [9]. This model considers the spatial channel and the environmental effects such as path-loss, frequency dependence, reflections, transmissions, and also diffractions. It considers as well the characteristics of the antennas as part of the effective channel such as directional gain, matching and polarization. A fair comparison has been carried out among three systems: the first uses two omnidirectional Half-Wave Dipole (HWD) antennas at each node, the second uses three directional antennas (horn antenna) at each transmitter node and two directional antennas (horn antenna) at each receiver node, in this system antenna selection (AS) technique is applied to select two antennas from the three at each transmitter. The third system uses two directional antennas at each node without AS (we choose the worst case in this manner). Fig. 2 shows a comparison between the three systems using the *average* BER vs. E_b/N_o for the whole multiuser system. As shown in Fig. 2 the artificial diversity technique improves the performance of the system significantly compared to the system that uses a HWD omnidirectional antennas and the other which uses the directional antennas without using AS. This figure proves that AS is a powerful technique to improve the BER performance of the system.
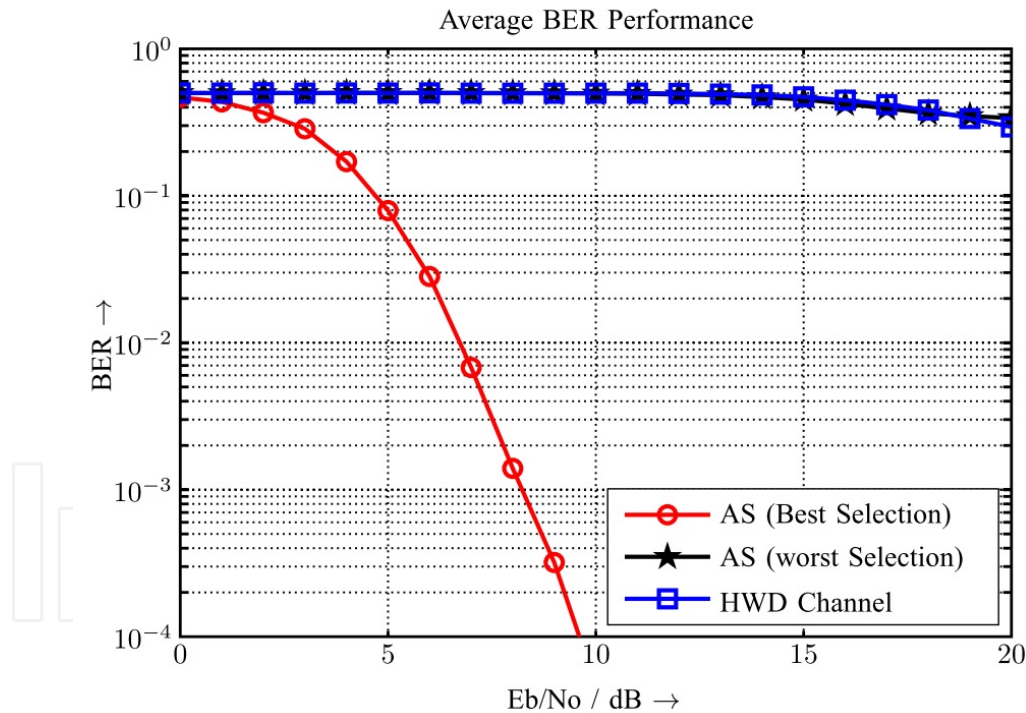

Figure 2. Comparison of average BER vs. Eb/No for a 3-user system by applying antenna selection (best and worst scenarios) and using omni-directional HWD antennas.

MIMO systems typically use antenna arrays and beamforming and spatial multiplexing. These beamforming methods do not result in (1) orthogonal channels nor (2) guarantee optimum data rates within the predefined environment e.g. indoors, outdoors, urban, suburban, etc. In designing optimal antenna systems, which fulfill the previously stated conditions, up to now, only heuristic methods have been employed. Presented here is a

systematic framework to fulfill the above 2 conditions, that aids in reducing the number of real world antennas to be used. The goal is to synthesize an optimal UWB antenna system which can be used by both the transmitter and receiver at any location within the investigated scenario. This synthesis method is based on [24] and has been used to design antennas for narrowband systems in [25]. The method is now extended to the design of UWB antenna systems. In the following sections, the theory and concepts behind this systematic synthesis will be given, followed by the methodology of realization and the results.

4. Spatial sampling with sampling antennas

The concept of 'spatial sampling' is presented in greater detail in [24, 30], but can be simplified to this: 'Given a predefined overall antenna aperture confined to a limited volume V, there exists a maximum spatial capacity limit with transmission system parameters i.e. antenna aperture size and element spacing. This can be determined by sampling the transmit and receive volumes with a set of ideal sampling antennas'. In a realistic case sampling antennas possess an overall aperture size and occupy a certain spatial volume. Therefore three parameters have to be considered for their design. First, the antenna aperture size, which will approximate the size of the real world antennas. The larger the aperture size, the higher the capacity, but this size is limited by the physical size of the desired real world antennas. Second, the minimum distance between the antenna elements in order to decrease their correlation [[18, 22]]. This parameter also influences the number of sampling antenna elements within the selected aperture size. It should be noted that the more elements the aperture contains, the more time is needed for the synthesis algorithm. Third, the frequency dependency of the previously mentioned parameters.
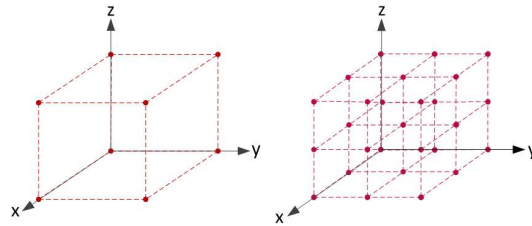

Figure 3. Sampling antenna configurations for spatial sampling, (left) minimum elements of 2×2×2, (right) more elements added, 3×3×3.

Here, a 5×5×5 cm^3 aperture based on the configuration in Fig. 3 has been chosen to illustrate the sampling antenna design and antenna synthesis algorithm in section 4.1. This configuration is then used in the subsequent antenna synthesis steps and the changes to the resulting radiation pattern over frequency is noted. If the resulting radiation pattern varies too much over frequency, the number of sampling antenna elements is then increased and the synthesis algorithm is repeated. This procedure is iterated until the resulting radiation pattern over frequency appear similar.

4.1. Channel diagonalization

For a time-invariant system, the transfer function is a transfer coefficient for all transmit and receive antenna pairs and can be expressed in the form of an $N \times M$-dimentional matrix **H**. Letting $\mathbf{y}_{\text{out}}$ be an $N \times 1$ matrix and $\mathbf{x}_{\text{in}}$ be an $M \times 1$ matrix with **n** as the noise vector, the received signal vector of a communication system can then be described in the frequency

domain as $\mathbf{y}_{\text{out}} = \mathbf{H}\mathbf{x}_{\text{in}} + \mathbf{n}$. Using singular value decomposition (SVD) $\mathbf{H}$ can be decomposed into $\mathbf{H} = \mathbf{USV}^{\dagger}$, where $\mathbf{S} = \mathbf{U}^{\dagger}\mathbf{HV}$ is a diagonal matrix whose elements are non-negative square roots of the eigenvalues λ_i of the matrix $\mathbf{HH}^{\dagger}$. $\mathbf{U}$ and $\mathbf{V}$ are unitary matrices, which fulfill the condition $(\mathbf{X}^{-1})^{\dagger} = \mathbf{X}$. Multiply the input vector $\mathbf{x}_{\text{in}}$ and the output vector $\mathbf{y}_{\text{out}}$ with the matrices $\mathbf{U}^{\dagger}$ and $\mathbf{V}$ respectively, and the original channel becomes and equivalent channel,

$$\hat{\mathbf{y}}_{\text{out}} = \mathbf{U}^{\dagger}\mathbf{y}_{\text{out}} = \mathbf{U}^{\dagger}(\mathbf{H}\mathbf{x}_{\text{in}} + \mathbf{n}) = \mathbf{U}^{\dagger}(\mathbf{HV}\hat{\mathbf{x}}_{\text{in}} + \mathbf{n}) = \mathbf{S}\hat{\mathbf{x}}_{\text{in}} + \hat{\mathbf{n}} \tag{25}$$

where $\hat{\mathbf{x}}_{\text{in}}$, $\hat{\mathbf{y}}_{\text{out}}$ and $\hat{\mathbf{n}}$ are the equivalent input, output and noise vectors respectively. The diagonal matrix $\mathbf{S}$ now becomes the channel matrix of the equivalent channel where each Eigenmode is interpreted as an independent SISO (single-input-single-output) subchannel and the capacity of the system becomes a sum over these SISO capacities as expressed by [12]

$$C = \sum_{i=1}^{K} \log_2 \left(1 + \frac{p_i \lambda_i}{\sigma_{\text{noise}}^2} \right) \tag{26}$$

with $K = \min(M, N)$, which is the rank of the matrix $\mathbf{HR_{xx}H}^{\dagger}$ with $\mathbf{R_{xx}}$ being the covariance matrix of the transmit signal, its Eigenvalues $\lambda_i(i = 1, 2, ..., K)$ and power coefficients $p_i(i = 1, 2, ..., K)$. From (26) the capacity of a MIMO system can be seen as a sum of independent K SISO subchannels (Eigenmodes) represented by the Eigenvalues λ_i, where each Eigenmode corresponds to one orthogonal subchannel. More explanation can be found in [16, 24].

Employing the waterfilling algorithm in the case of channel state information (CSI) known to the transmitter will result in an optimum capacity solution for such a MIMO channel. The $\mathbf{U}$ and $\mathbf{V}$ matrices are called the 'beamforming matrices' as they determine the mapping and weighting of all the signals onto the antenna elements.

5. Scenario-based MIMO antenna synthesis

In order to apply the SVD technique to obtain parallel subchannels, the channel matrix $\mathbf{H}$ of the intended scenario must be provided. One of the most reliable and repeatable way of obtaining the SISO channel matrix $\mathbf{H}$ is through ray-tracing with the software developed by [10]. The ray-tracing simulations are done in parallel with the design of the sampling antenna configuration.

A typical indoor scenario (with glass windows, furniture, ceiling and floor) was built for simulation as shown in Fig. 4. The size of the room is $10 \times 10 \times 3$ m and simulations were done for transmitters and receivers at randomized positions in the room with an antenna height 1.5 m over the frequency band of 3.1 GHz to 10.6 GHz. Omni-directional antennas (dipoles) are used, along with the option of using both vertical and horizontal polarizations for an added degree of freedom for the design of the real world antenna. Around 45600 random transmitter-receiver points were simulated in order to acquire a synthesis result, that when the averaging strategies in section 6 have been applied, will be applicable from virtually any point in the intended scenario.
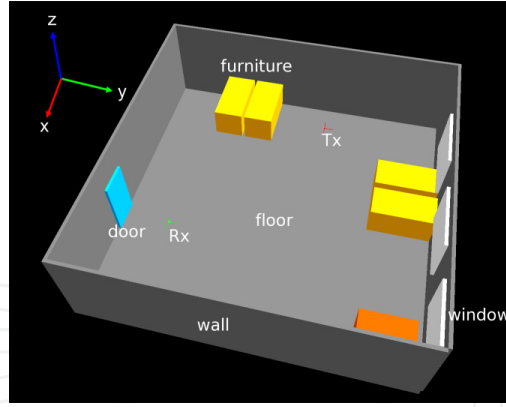
Figure 4. Indoor scenario for ray-tracing

5.1. SISO to MIMO extrapolation

A complete characterization of the MIMO channel matrix with ray-tracing requires $N \times M$ runs taking into account the sampling antenna configuration, which is computationally inefficient. [11] presents a method to reduce the calculation effort by assuming that the same plane wave impinges on all sampling antenna elements. Since the sampling antenna elements spacing is small and fixed, the difference of the incident wave at the origin of the sampling antenna configuration shown in Fig. 3 with the other antenna elements is only the phase difference expressed as

$$\Delta \varphi_i = -\beta \left(\Delta x_i \sin \vartheta \cos \psi + \Delta y_i \sin \vartheta \sin \psi + \Delta z_i \cos \vartheta \right) \tag{27}$$

where ϑ and ψ are the angles of arrival or departure of the incident wave in elevation and azimuth respectively. Hence the SISO to MIMO extrapolation reduces the computation of the MIMO **H** matrix to only one SISO run.

5.2. Antenna system simplification

In order to simplify the system, a plot of the eigenvalues (obtained after the SVD) versus the frequency is used to identify the channels with the strongest power. For instance, if only the first two subchannels were identified as having significant power as compared to the rest, the beamforming matrices **U** and **V** can be modified to contain only those two subchannels. With this, the system will now comprise only 2 inputs and 2 outputs.

6. Synthesis results

The resulting synthesized antenna radiation patterns for both the transmitter and receiver at one point for several different frequencies are as shown in Fig. 5. The figure shows the 3D plot of the radiation patterns for two subchannels and is computed using:

$$\vec{E}(d, \vartheta, \psi) = \vec{E}_{\text{single}}(d, \vartheta, \psi) \cdot \frac{e^{-j\beta d}}{d} \cdot \sum_{i=1}^{N_{\text{ant}}} a_i \, e^{-j(\beta(d_i - d) + \zeta_i)} \tag{28}$$

where $\vec{E}_{\text{single}}$ is the electric field of the sampling antenna used (a dipole in this case), N_{ant} is the total number of transmitter or receiver antennas (since they both use the same sampling antenna configuration), β is the wave number, d is the distance from the origin of the sampling antenna to a far-field observation point, $a_i \angle \zeta_i$ is the weighting from the **U** and **V** beamforming matrices, $d_i - d = \Delta\varphi$ in (27) and $\Delta x_i, \Delta y_i, \Delta z_i$ are the position of the individual elements in the array according to the Cartesian coordinate system.
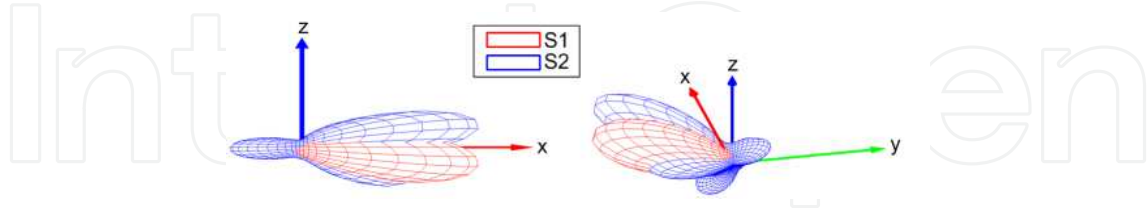

Figure 5. Resulting synthesized antenna radiation pattern for a transmit-receive pair (horizontal polarization) for subchannel 1 (S1), with line-of-sight propagation, and subchannel 2 (S2), with propagation paths reflected from the ceiling and floor, for the aperture size $5\times5\times5\,\text{cm}^3$ with $5\times5\times5$ elements, (left) side view and (right) bottom view. (Image taken from [29])

Averaging strategy

Three averaging strategies were used, namely averaging over frequency, over location, and of transmitter and receiver radiation patterns. The first averages all radiation patterns obtained at frequency points between 3.1 to 10.6 GHz to obtain a pattern which is valid for the UWB. The second averages the radiation pattern obtained from random points around the scenario so that the resulting radiation pattern is valid for use in the whole scenario. The third averaging is done if the resulting transmitter and receiver radiation patterns look qualitatively similar, so that both can use the same antennas.

6.1. Capacity analysis

The capacity for the averaged synthesized patterns according to the number of sampling antennas across the ECC (Electronic Communications Committee) standard's UWB band was analyzed using (26). The term p_i is taken from the power spectral density levels of the ECC UWB spectral mask, λ_i is the Eigenvalue of the subchannel from the matrix **S** and $\sigma^2_{\text{noise}} = kTB$, where k is the Boltzmann constant, $T = 297\,\text{K}$ and $B = 100\,\text{MHz}$. Fig. 6 shows the capacity of the synthesized radiation pattern using $2\times2\times2$ till $5\times5\times5$ sampling antenna elements within the defined $5\times5\times5\,\text{cm}^3$ physical space. It can be seen that the higher the number of sampling antennas, the more the capacity increases, agreeing with the theory in [18]. Noting that the rise in the capacity is decreasing with the higher element configuration used, we conclude that the $5\times5\times5$ configuration is nearing the capacity saturation limit.

7. Real world antennas

The real world antennas which match the elevation characteristics over frequency of the optimized synthesized antennas can be found in [1]. Two dual orthogonal polarized antennas are used along with a 180° hybrid coupler to form the two subchannels. The comparison of the radiation pattern over frequency of the synthesized antennas and the real world antennas is shown in Fig. 7 .
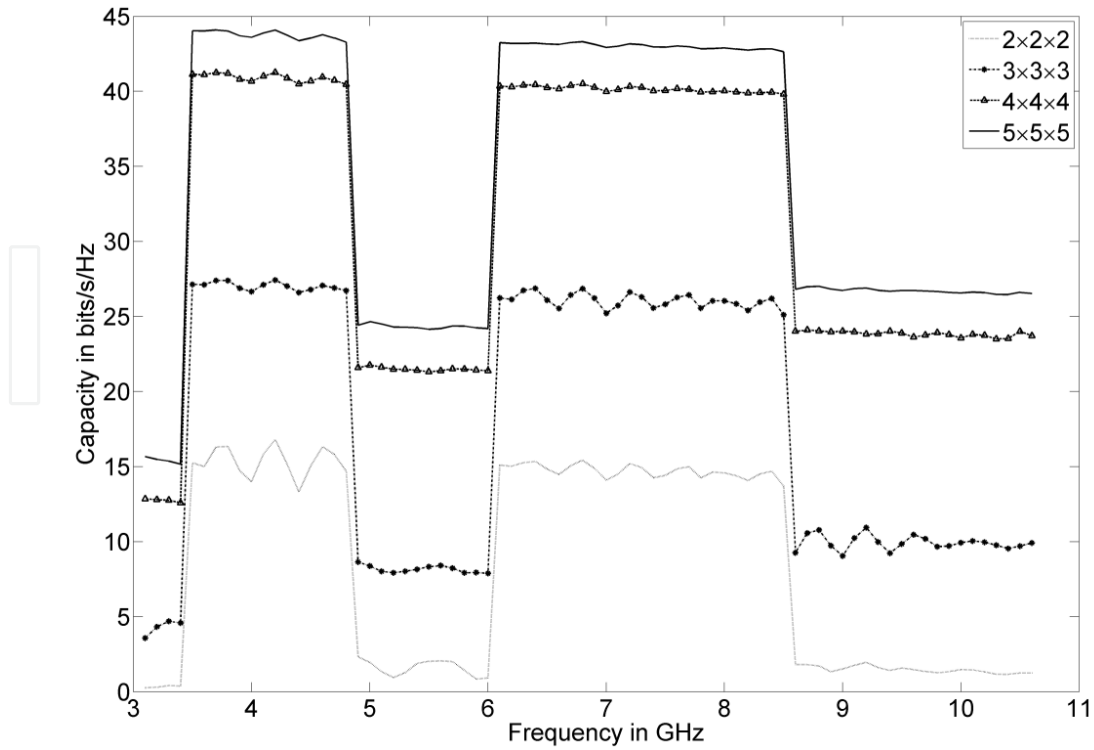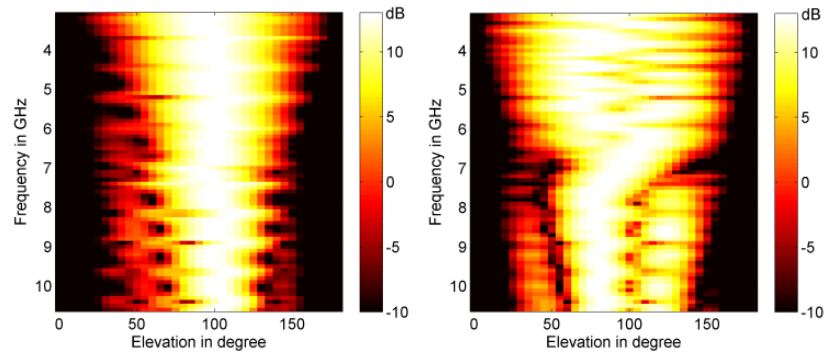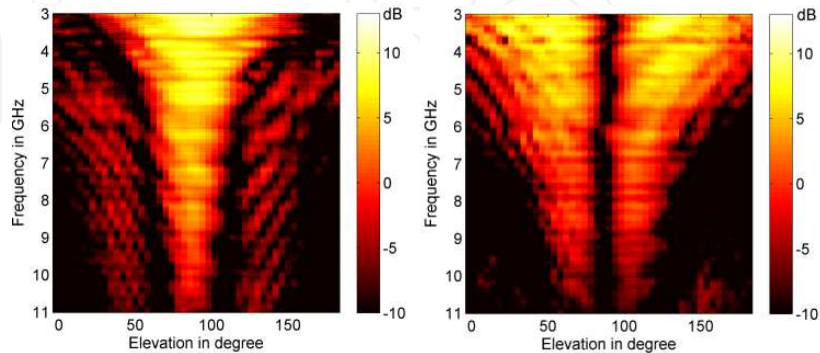
Figure 6. Capacity analysis for the aperture size $5\times5\times5\,\text{cm}^3$. (Image taken from [29])

(a) Synthesized antennas, (left) subchannel 1 (right) subchannel 2

(b) Real world antennas (left) subchannel 1 (right) subchannel 2

Figure 7. Synthesized antennas vs. real world antennas: radiation pattern (elevation) over frequency

7.1. Orthogonal channels multimode antenna selection criteria

Before the above mentioned real world UWB antennas are used, the IA algorithm is tested with a narrowband multimode antenna with orthogonal channels. The narrowband antenna system is designed for use at 5.9 GHz to 6.15 GHz, consisting of four monopoles built on a finite ground plane as shown in Fig. 8(a). This antenna system is capable of radiating four different orthogonal modes based on the amplitude and phase of the excitation signals to the antenna ports. More details about this antenna can be found in [15].

Two modes as shown in Fig. 8(c) and (d) were chosen and the antenna system was simulated with a ray-tracing software within the scenario shown in Fig. 8(b). The simulation has been performed for 1000 different transmit and receive nodes locations. Simulation results shown in Fig. 9 illustrates that the overall BER system performance has been significantly improved with the multimode antenna system compared to the half wave dipoles (HWD). That is due to the additional path diversity to the communication system.
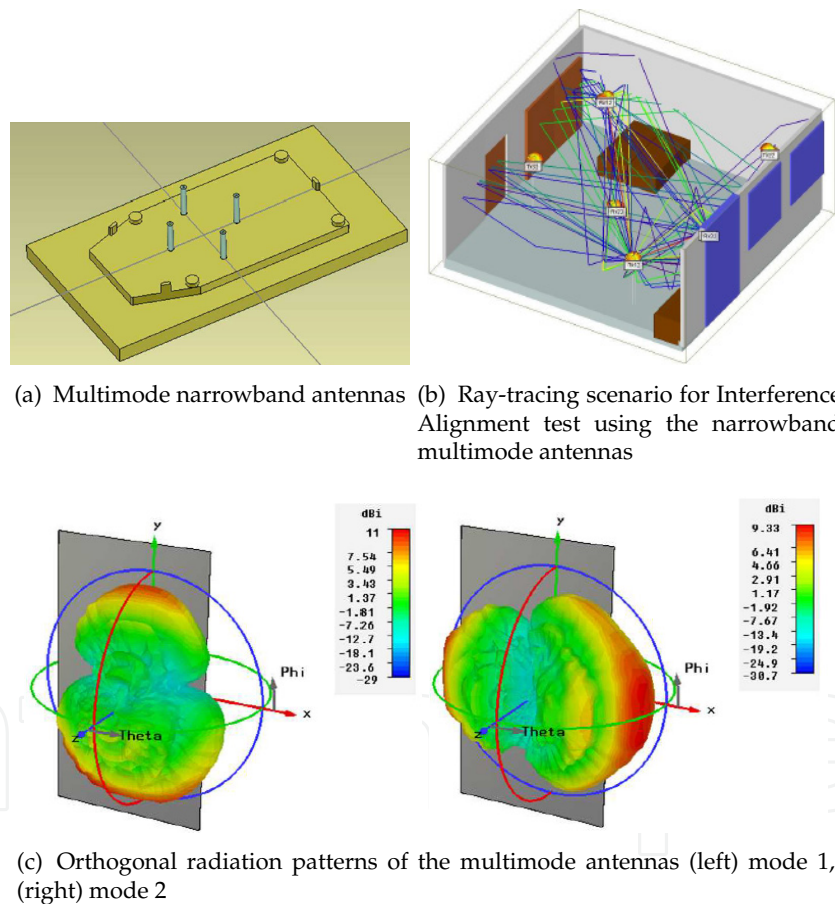

(a) Multimode narrowband antennas (b) Ray-tracing scenario for Interference Alignment test using the narrowband multimode antennas

(c) Orthogonal radiation patterns of the multimode antennas (left) mode 1, (right) mode 2

Figure 8. Multimode narrowband antennas for preliminary Interference Alignment algorithm analysis

8. Hardware requirements of IA systems

High throughput wireless communication systems including LTE, ECMA-368 (WiMedia) and IEEE 802.11ac are built around sophisticated digital signal processing algorithms. Among the research goals for future communication standards are higher spectral efficiency, higher
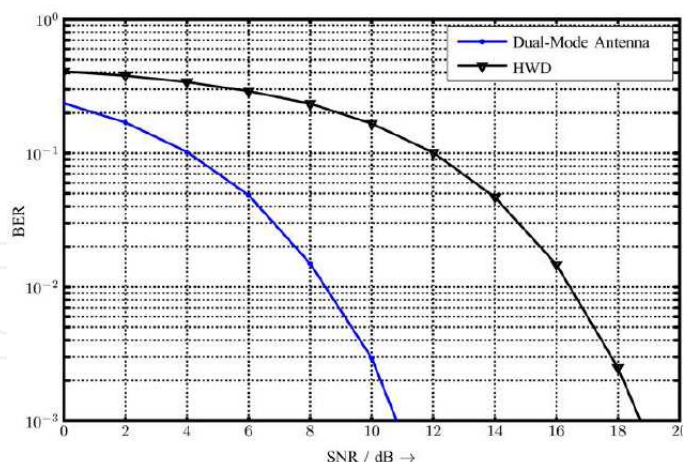
Figure 9. Comparison of the average BER vs. E_b/N_o of the IA system by applying multimode antenna systems and comparing to HWDs.

energy efficiencies towards the Shannon limit and increased data rates. Naturally, these benefits come at the price of higher computational complexity. The demand for flexible realtime hardware platforms capable of delivering the required huge number of operations per second at a severely limited power and silicon area budget has led to the development of specialized hardware platforms for software defined radio (SDR) applications. Techniques from FPGA-based ASIC verification and rapid prototyping are combined in this project for the design space exploration of highly optimized hardware architectures.

In a typical implementation scenario for complex designs, high level reference models are used. The choice of optimization-blocks is often based on profiling results, with those blocks contributing significantly to the overall resource requirements being chosen for optimization. This leads to a hybrid design consisting of a mixture of high level blocks and highly optimized blocks, running on hardware ranging from general purpose processors (GPP), application specific instruction set processors, FPGA-based rapid prototyping systems and dedicated hardware accelerators. The presented design space exploration framework reflects this structure and allows the designer to freely move processing blocks between the different layers of optimization.

The design space exploration framework created within this project is presented in Section 8.2. A hardware implementation case study of a closed-form 3-user IA algorithm has been selected for presentation in Section 8.3. Cost functions for an iterative IA algorithm are given in Section 8.4.

8.1. Wireless communication systems design space exploration

The process of designing complex digital electronic circuits offers a large variety of options to the designer. There are many valid possible implementations that fulfill the specification, but they differ in certain properties, e.g. silicon area, power efficiency, flexibility, testability and design effort. These properties span the so-called design space. A design space exploration establishes relations between possible points in the design space, ultimately leading to cost functions modeling the relation between the design properties and parameters. These models serve as a quantitative basis to make important design decisions in an early design phase.

Certain parameters are of special interest in the domain of wireless communication platforms. The limited power budget in mobile devices puts hard constraints on the power efficiency, requiring power optimization across all layers of algorithm development, design implementation and semiconductor technology.

Deriving comprehensive cost models using Monte-Carlo methods requires visiting a significantly larger number of points in the design space compared to existing heuristically driven parameter optimization approaches covered by existing FPGA-based simulation acceleration systems. The achievable simulation speedup is a key factor enabling the characterization and optimization of complex communication systems using Monte-Carlo approaches which are infeasible for pure software simulation due to the large required stimuli sets.

8.2. Development framework

The FPGA-based hybrid hardware-in-the-loop research and design space exploration (DSE) framework created in this work combines high-level tools (e.g. MATLAB/Simulink) and optimized hardware blocks [17]. Its application domain ranges from the design, optimization and verification of efficient and optimized signal processing blocks for computationally demanding next-generation wireless communication systems to system characterization and DSE.
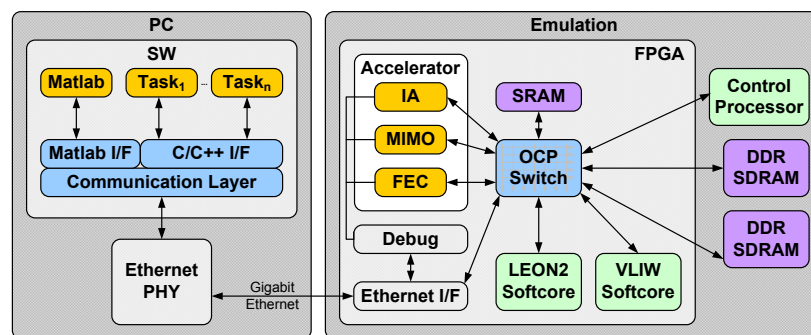

Figure 10. Emulation framework block diagram

The framework consists of a host PC, FPGA-based emulation systems, a generic fully synthesizeable VHDL SoC infrastructure, dedicated processors, processor softcores and a software library providing a transparent communication application programming interface (API). This allows signal processing blocks to be split and run distributed on a highly heterogeneous signal processing system. Software API libraries provide unified transparent communication between MATLAB, C/C+, embedded software and the hardware on-chip multilayer bus system. The same resources are accessible from all components, enabling a flexible partitioning and migration of processing task between high-level software, embedded software and dedicated hardware modules. The framework block diagram is shown in Figure 10. The properties of the optimized on-chip infrastructure template make it suitable for usage in final ASIC targets and thus enable the test, debugging and characterization of signal processing blocks in their target environment. Using standard FPGA design flows, new computationally intensive processing cores are directly implemented as the optimized hardware target modules. Instrumentation is used to enable dynamic, software controlled parameter adjustment. The remaining blocks may continue to run as high-level models,

enabling a divide-and-conquer implementation and verification approach. The framework provides transparent data transport between the substituted MATLAB modules and multiple parallel instances of their FPGA hardware counterparts. The same interfaces are available for hardware simulation via the Modelsim foreign language interface (FLI), effectively also providing a verification and debugging environment at minimal extra effort.

The PC is connected to the emulation systems via Gigabit Ethernet. The generic FPGA infrastructure template comprises an OCP multilayer bus, the ethernet DMA interface, SDRAM controllers, on-chip memories and massively parallel parameterized softcore processors [20]. It has been adapted to and tested on a Xilinx Virtex-6 LX550T based BEE4 rapid prototyping system, the Xilinx Virtex-6 ML605 Evaluation Kit and the Virtex-5 LX220 based MCPA board [2] developed at IMS, see Fig. 11.
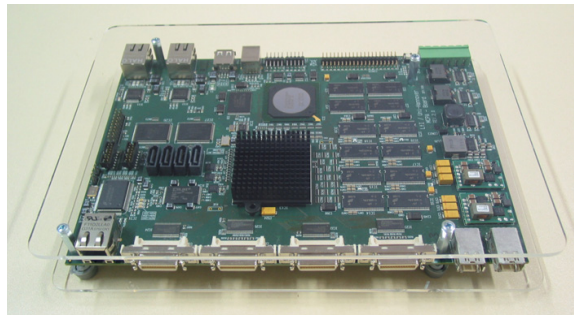

Figure 11. FPGA-based emulation system developed at IMS

8.3. Case study: 3-user antenna selection interference alignment

An implementation of the antenna selection interference alignment algorithm presented in Section 3 has been chosen as a case study using the development framework presented in Section 8.2. The proposed 3-user 2x2 MIMO zero-forcing IA antenna selection algorithm computes precoding matrices $\mathbf{V}$, decoding matrices $\mathbf{U}$ and a metric η based on [4]. Compared to the experimental testbed for fixed antenna patterns presented in [13], our implementation also chooses a subset of channels (i.e. antennas or radiation patterns) from the available channels. This leads to an increased channel orthogonality for the chosen channels at a reduced number of RF front ends.

The problem of finding the optimum antenna combination $\hat{i}$ from a set of I combinations can be formulated as

$$\hat{i} = \arg\max_{i=1...I} \sum_{k=1}^{K} \eta(\mathbf{V}_{k,i}, \mathbf{U}_{k,i}) \tag{29}$$

where $\eta(\mathbf{V}, \mathbf{U})$ is a function of the resulting SNR according to Section 3.1. $\mathbf{V}_{k,i}$ and $\mathbf{U}_{k,i}$ are the precoding and decoding matrices of user k for a given antenna combination i. Equation 29 is solved by visiting all I antenna combinations.

8.3.1. Computational complexity

The resource requirements of an optimized efficient integer implementation of the proposed novel antenna-selection IA algorithm is presented in this section, based on FPGA implementation results. Target systems include SDR platforms, FPGAs and ASICs.

This section focuses on the costs of the 3-user 2x2 MIMO processing consisting of matrix inversions, matrix multiplications, eigenvector computation and normalization, see Equations 6 to 9. The metric η is computed for both eigenvectors. All intermediate matrices can be independently scaled by arbitrary scalars without affecting the antenna decision or **V** and **U**. Exploiting this makes the cost of all involved 2x2 matrix inversions negligible and allows intermediate matrices to be block-normalized by shifting, i.e. extract a common power of 2 from all matrix elements. This results in reduced integer word lengths and thus reduced hardware costs. Table 1 summarizes the number of required real-valued mathematical base operations for antenna selection and the computation of **V** and **U** per antenna combination and subcarrier, without a final normalization step of **V** and **U**. Complex multiplications are composed of three real multiplications, three additions and two subtractions, `INVSQRT` denotes the reciprocal square root [26].

OP	ADD	MUL	SQRT	INVSQRT
Matrix mult.	696	348	0	0
Eigenvectors	15	8	3	0
Metric score	46	82	6	2
#OPC	757	438	9	2

Table 1. Operation counts for the computation of η per antenna combination i and subcarrier

To keep the total transmit power constant, the chosen antenna combination's precoding matrices V need to be normalized, resulting in 3 `ADD`, 8 `MUL` and 1 `INVSQRT` additional operations #OPN per transmitter and subcarrier. The above analysis implies that in general, the implementation cost is dominated by the multiplications in terms of silicon area and power consumption.

For the case of $K = 3$ users with $M = 2$ active transmit antennas used out of $L = 3$ physical antennas per transmitter and $N = 2$ antennas per receiver, there are 27 antenna combinations to be visited per subcarrier.

For realtime operation, the maximum allowable latency is defined to be T_0. Assigning relative operation costs α_i to each operation type OP_i, the total computational cost C for S subcarriers becomes

$$C = \frac{S}{T_0} \cdot \left(n \cdot \sum_{i \in OP} \alpha_i \cdot \#OPC_i + K \cdot \sum_{i \in OP} \alpha_i \cdot \#OPN_i \right) \qquad (30)$$

8.3.2. Hardware cost estimation

Using α as relative silicon area costs, the total silicon area implementation cost of an architecture without resource sharing can be estimated from Eq. (30). The relative area α of 16-bit arithmetic operations for an ASIC implementation based on [23] results in the values given in Table 2. The relative costs α_{MUL} of a multiplier are defined to be 1.

OP	ADD	MUL	SQRT	INVSQRT
α	0.108	1	1.73	3

Table 2. Relative silicon area costs of 16-bit arithmetic operations

For a system using antenna selection at the transmitter only with $L = 3$ antennas, $S = 128$ subcarriers and $T_0 = 1\,\text{ms}$, the total IA costs are estimated to be $C = 1.875\,\text{GOPS}$.

For the configuration above, the original MATLAB algorithm takes 3.63 s on an Intel Xeon 2.4 GHz CPU running MATLAB R2012a for the computation of the optimal antenna combination $\hat{i}$ and its corresponding precoding and decoding matrices V_k and U_k from a set of channel information H. The FPGA implementation created in this case study achieves realtime operation, requiring 380 μs at 100 MHz clock frequency on a Xilinx Virtex-6 LX550T FPGA in a BEE4 emulation system. Thus, the achieved speedup is 9553.

8.4. Cost functions for K-user IA

The implementation presented in the previous section is a based on a closed-form $K = 3$ user IA algorithm. There is no known closed-form solution for $K > 3$ users, but iterative algorithms exist. In this section, we present implementation complexity estimates of the minimum mean square error (MMSE) IA algorithm presented in [27].
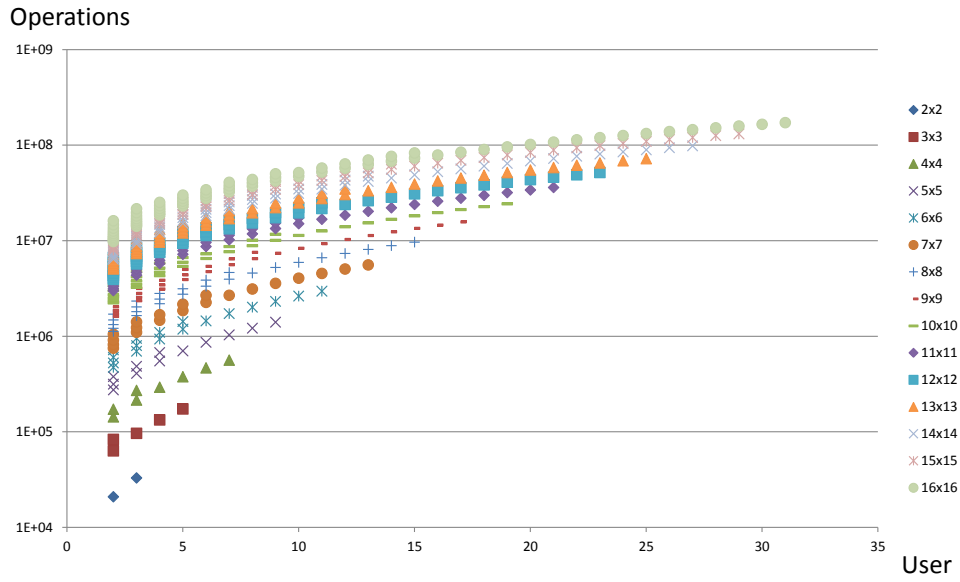

Figure 12. Number of operations for iterative MMSE interference alignment (4 iterations)

The MMSE-IA algorithm starts with arbitrary precoding matrices $\mathbf{V}_k$, then iteratively updates the decoding and precoding matrices $\mathbf{U}_k$ and $\mathbf{V}_k$ according to Eq. (31) and (32) until convergence. The Lagrange multiplier $\lambda_k \geq 0$ is computed to satisfy $\|\mathbf{V}_k\|_2^2 \leq 1$ by Newton iteration.

$$\mathbf{U}_k = \left(\sum_{j=1}^{K} \mathbf{H}_{kj} \mathbf{V}_j \mathbf{V}_j^H \mathbf{H}_{kj}^H + \sigma^2 \mathbf{I} \right)^{-1} \mathbf{H}_{kk} \mathbf{V}_k \tag{31}$$

$$\mathbf{V}_k = \left(\sum_{j=1}^{K} \mathbf{H}_{jk}^H \mathbf{U}_j \mathbf{U}_j^H \mathbf{H}_{jk} + \lambda_k \mathbf{I} \right)^{-1} \mathbf{H}_{kk}^H \mathbf{U}_k \tag{32}$$

The number of required iterations is data-dependent. Each iteration step requires the following operations to be executed: matrix multiplication, pseudo-inverse, Newton

iterations. Figure 12 summarizes the estimated number of operations for the computation of a set of **V** and **U** matrices, based on well-known optimized hardware implementations. Comparing the iterative approach computational complexity to the the closed-form 2x2 IA implementation presented in Section 8.3, the number of operations is increased by a factor of approximately 60.8.

9. Conclusion

IA is a promising approach for communications with numerous pairs of users. In our contribution we have investigated the usefulness of IA for MIMO UWB communication systems. Beside apart of the significant power processing needed for the high data rate applications, the MIMO UWB antenna design remains a challenge. The antenna synthesis presented here can be viewed as synthesizing an antenna system with optimal radiation pattern catered towards an intended scenario. This antenna system radiates orthogonalized channels (after the averaging strategies) with sufficient power and has fixed beamforming (direction optimized according to the scenario and with averaging over various positions) at the transmitter and receiver antenna systems. Also, the resulting system has been simplified to 2 inputs and 2 outputs based on the subchannels with the strongest power. The whole system has been simulated by an indoor ray tracing tool and the corresponding MIMO UWB base band modulation schemes and detection techniques. Moreover, an antenna selection method is proposed in order to increase the robustness of IA in real environments. It is demonstrated that by using orthogonal multimode antennas a significant gain can be obtained. In the third and last part of our contribution the hardware efforts of IA algorithms are studied in more detail. It is worked out that highly challenging system blocks like IA can be elaborated today only by the help of suitable hardware emulation platforms which are typically FPGA-based. Therefore, a generic methodology has been elaborated and implemented which allows to explore the implementation design space. The hybrid hardware-in-the-loop research and design space exploration (DSE) framework created in this work combines high-level tools (e.g. Matlab/Simulink) and optimized hardware blocks. The properties of the elaborated optimized on-chip infrastructure template make it suitable for usage in final ASIC targets and thus enable the test, debugging and characterization of signal processing blocks in their target environment. This DSE framework has been used to derive cost models for K-user iterative IA algorithms. Estimates for the implementation effort (e.g. in terms of operation counts in dependency of the number of users) have been derived. Because of this project, a generic DSE framework is available and can be used to work out suitable architectures for further challenging building blocks.

Author details

Mohamed El-Hadidy, Mohammed El-Absi and Thomas Kaiser
Duisburg-Essen University, Institute of Digital Signal Processing (DSV), Germany

Yoke Leen Sit and Thomas Zwick
Karlsruhe Institute of Technology, Institut für Hochfrequenztechnik und Elektronik (IHE), Germany

Markus Kock and Holger Blume
Leibniz Universität Hannover, Institute of Microelectronic Systems (IMS), Germany

10. References

[1] Adamiuk, G. [2010]. *Methoden zur Realisierung von Dual-orthogonal, Linear Polarisierten Antennen für die UWB-Technik*, PhD thesis, Karlsruhe.
URL: *http://digbib.ubka.uni-karlsruhe.de/volltexte/1000019874*

[2] Banz, C., Hesselbarth, S., Flatt, H., Blume, H. & Pirsch, P. [2012]. Real-Time Stereo Vision System using Semi-Global Matching Disparity Estimation: Architecture and FPGA-Implementation, *Transactions on High-Performance Embedded Architectures and Compilers, Springer* .

[3] Björck, Å. & Golub, G. H. [1973]. Numerical methods for computing angles between linear subspaces, *Math. Comp.* 27: 579–594.

[4] Cadambe, V. & Jafar, S. [2008]. Interference alignment and degrees of freedom of the k -user interference channel, *Information Theory, IEEE Transactions on* 54(8): 3425 –3441.

[5] Cadambe, V. & Jafar, S. [2009]. Reflections on interference alignment and the degrees of freedom of the k-user mimo interference channel, *IEEE Information Theory Society Newsletter* 54(4): 5 –8.

[6] El-Absi, M., El-Hadidy, M. & Kaiser, T. [2012]. Antenna selection for interference alignment based on subspace canonical correlation, *2012 International Symposium on Communications and Information Technologies (ISCIT)* .

[7] El Ayach, O., Peters, S. & Heath, R. [2010]. The feasibility of interference alignment over measured mimo-ofdm channels, *Vehicular Technology, IEEE Transactions on* 59(9): 4309 –4321.

[8] El-Hadidy, M., El-Absi, M. & Kaiser, T. [2012]. Articial diversity for uwb mb-ofdm interference alignment based on real-world channel models and antenna selection techniques, *2012 IEEE International Conference on Ultra-Wideband (ICUWB)* .

[9] El-Hadidy, M., Mohamed, T., Zheng, F. & Kaiser, T. [2008]. 3d hybrid em ray-tracing deterministic uwb channel model, simulations and measurements, 2: 1 –4.

[10] Fügen, T., Maurer, J., Kayser, T. & Wiesbeck, W. [2006]. Capability of 3-D Ray Tracing for Defining Parameter Sets for the Specification of Future Mobile Communications Systems, *Antennas and Propagation, IEEE Transactions on* 54(11): 3125 –3137.

[11] Fügen, T., Waldschmidt, C., Maurer, J. & Wiesbeck, W. [2003]. MIMO capacity of bridge access points based on measurements and simulations for arbitrary arrays, *5th European Personal Mobile Communications Conference*, pp. 467–471.

[12] Gesbert, G., Shafi, M., Shiu, D., Smith, P. J. & Naguib, A. [2003]. From Theory to Practice: An Overview of MIMO Space-Time Coded Wireless Systems, *IEEE Journal on Selected Areas in Communications* 21: 281–302.

[13] González, O., Ramírez, D., Santamaría, I., García-Naya, J. & Castedo, L. [2011]. Experimental validation of interference alignment techniques using a multiuser MIMO testbed, *Smart Antennas (WSA), 2011 International ITG Workshop on*, pp. 1 –8.

[14] Heath, R., Sandhu, S. & Paulraj, A. [2001]. Antenna selection for spatial multiplexing systems with linear receivers, *IEEE Commun. Letters* 5(4): 142 –144.

[15] Jereczek, G. [2010]. *Design of Capacity Maximizing MIMO Antenna Systems for Car-2-Car Communication*, Master's thesis, Karlsruhe Institute of Technology (KIT), Karlsruhe, Germany.

[16] Khalighi, M. I., Brossier, J., Jurdain, G. & Raoof, K. [2001]. Water Filling Capacity of Rayleigh MIMO Channels, *IEEE Transactions on Antennas and Propagation* 1: A155–A158.

[17] Kock, M., Hesselbarth, S. & Blume, H. [2013]. Hardware-accelerated design space exploration framework for communication systems, *Wireless Innovation Forum Conference*

on Wireless Communications Technologies and Software Defined Radio (SDR-WInnComm 2012), Washington, DC, USA. Accepted for publication.

[18] Loyka, S. & Mosig, J. [2006]. *Information Theory and Electromagnetism: Are They Related?*, CRC Press.

[19] Molisch, A., Win, M. & Winters, J. [2001]. Capacity of mimo systems with antenna selection, *IEEE International Conference on Communications (ICC)* (4): 570 –574.

[20] Paya-Vaya, G. & Blume, H. [2012]. TUKUTURI: A dynamically reconfigurable multimedia soft-processor for video processing applications, *Poster presentation at the 7th International Conference on High-Performance and Embedded Architectures and Compilers, HiPEAC'12, Paris, France*, Vol. USB Proceedings.

[21] Peters, S. & Heath, J. [2009]. Interference alignment via alternating minimization, *Int. Conf. on Acoust. Speech and Signal Processing,(ICASSP)* .

[22] Petersen, D. P. & Middleton, D. [1962]. Sampling and Reconstruction of Wave-limited functions in N-dimensional Euclidean Spaces, *Information and Control* 5: 279 – 323.

[23] Pirsch, P. [1998]. *Architectures for Digital Signal Processing*, John Wiley & Sons, Inc.

[24] Pontes, J. [2010]. *Optimized Analysis and Design of Multiple Element Antenna for Urban Communication*, Karlsruher Institut fuer Technologie (KIT).

[25] Reichardt, L., Pontes, J., Sit, Y. & Zwick, T. [2011]. Antenna optimization for time-variant mimo systems, *Antennas and Propagation (EUCAP), Proceedings of the 5th European Conference on*, pp. 2569 –2573.

[26] Salmela, P., Burian, A., Järvinen, T., Happonen, A. & Takala, J. H. [2011]. Low-complexity inverse square root approximation for baseband matrix operations, *ISRN Signal Processing* vol. 2011.

[27] Schmidt, D., Shi, C., Berry, R., Honig, M. & Utschick, W. [2009]. Minimum mean squared error interference alignment, *Signals, Systems and Computers, 2009 Conference Record of the Forty-Third Asilomar Conference on*, pp. 1106 –1110.

[28] Shen, M., Zhao, C., Liang, X. & Ding, Z. [2011]. Best-effort interference alignment in ofdm systems with finite snr, *IEEE International Conference on Communications (ICC)* 2(4): 5 –9.

[29] Sit, Y. L., Reichardt, L., Liu, R., Liu, H. & Zwick, T. [2012]. Maximum Capacity Antenna Design for an Indoor MIMO-UWB Communication System, *10th International Symposium on Antennas, Propagation and EM Theory, Xian, China*.

[30] Wallace, J. W. & Jensen, M. A. [2002]. Intrinsic Capacity of the MIMO Wireless Channel, *IEEE Proceedings of the 56th Vehicular Technology Conference VTC 2002-Fall*, pp. 701–705.